



1 **Measurement report: Changes in light absorption and molecular**
2 **composition of water-soluble humic-like substances during a winter**
3 **haze bloom-decay process in Guangzhou, China**

4
5 Chunlin Zou^{1,3}, Tao Cao^{1,3}, Meiju Li^{1,3}, Jianzhong Song^{1,2,4,*}, Bin Jiang^{1,2}, Wanglu Jia^{1,2},
6 Jun Li^{1,2}, Xiang Ding^{1,2}, Zhiqiang Yu^{1,2,4}, Gan Zhang^{1,2}, Ping'an Peng^{1,2,3,4}

7 ¹State Key Laboratory of Organic Geochemistry and Guangdong Provincial Key
8 Laboratory of Environmental Protection and Resources Utilization, Guangzhou Institute
9 of Geochemistry, Chinese Academy of Sciences, Guangzhou 510640, China

10 ²CAS Center for Excellence in Deep Earth Science, Guangzhou 510640, China

11 ³University of Chinese Academy of Sciences, Beijing 100049, China

12 ⁴Guangdong-Hong Kong-Macao Joint Laboratory for Environmental Pollution and
13 Control, Guangzhou 510640, China

14

15 **Correspondence to:* Jianzhong Song (songjzh@gig.ac.cn)

16

17



18 **Abstract**

19 Water-soluble humic-like substances (HULIS) absorb light in near-UV and visible
20 wavelengths and exert significant influence on the atmospheric environment and climate.
21 However, knowledge on HULIS evolution during haze bloom-decay process is limited.
22 Herein, PM_{2.5} samples were obtained during a winter haze event in Guangzhou, China,
23 and light absorption and molecular composition of HULIS were investigated by UV-vis
24 spectrophotometry and ultrahigh-resolution mass spectrometry. Compared with HULIS
25 in clean days, the absorption coefficients (Abs₃₆₅) of HULIS in haze days were
26 significantly higher but the mass absorption efficiencies (MAE₃₆₅) were relatively lower,
27 suggesting diverse and dynamic absorption properties of HULIS during haze episodes.
28 The CHO and CHON compounds were the most abundant components in HULIS,
29 followed by CHOS, CHONS, and CHN. Haze HULIS presented comparatively higher
30 molecular weight, lower aromaticity index (AI_{mod}), and higher O/C_w, O/N_w, and O/S_w
31 ratios, indicating that HULIS fractions undergo relatively higher oxidation during haze
32 days than clean days. Moreover, CHON and CHO compounds with high AI_{mod} were the
33 major potential chromophores in HULIS and significantly contributed to HULIS light
34 absorption. It's worth noting that the proportions of these chromophores were decreased
35 during haze event, mainly owing to their higher oxidation and longer aging period during
36 haze episode. Besides, accumulated contribution of organic compounds emitted from
37 vehicles and formed from stronger reactions of bio-VOCs also diluted light-absorbing
38 compounds in haze HULIS. These findings help to understand HULIS evolution during
39 haze bloom-decay process in the subtropic region of China.

40



41 **1. Introduction**

42 Water-soluble humic-like substances (HULIS), belonging to a class of highly
43 complex organic compounds with physical/chemical properties similar to humic
44 substances in natural environments, which constitute 30%–70% of water-soluble organic
45 compounds in ambient aerosols and are responsible for > 70% of light absorption in
46 water-soluble brown carbon (BrC) (Graber and Rudich, 2006; Laskin et al., 2015; Huang
47 et al., 2018). HULIS are ubiquitously identified in atmospheric aerosols, fog, cloud, and
48 rain water, and have been demonstrated to play significant effects on both atmospheric
49 environment and climate (Bianco et al., 2018; Wu et al., 2018b; Zeng et al., 2021). In
50 addition, HULIS exert adverse health effects because they can enhance the oxidative
51 potential of organic aerosols (Ma et al., 2019; Wong et al., 2019; Chen et al., 2019).

52 In recent years, severe particulate pollution (i.e., haze events) frequently occur in
53 some developing country such as China, which has drawn extensive public and scientific
54 concerns (Huang et al., 2014; Wang et al., 2014; An et al., 2019; Zhang et al., 2020).
55 According to An et al. (2019), contributions of organic aerosols, including primary
56 organic aerosols and secondary organic aerosols (SOA), are significant for severe haze
57 events; in particular, the contribution of SOA in China is expected to continuously
58 increase because of stronger chemical reactions in the atmosphere (An et al., 2019).
59 HULIS are an important component in organic aerosols, which originate from a variety of
60 primary emissions (e.g., biomass burning (BB), coal combustion, off-road engine
61 emission) (Fan et al., 2016; Cui et al., 2019; Tang et al., 2020) and secondary chemical
62 oxidation of biogenic and anthropogenic volatile organic compounds (VOCs) (Rincón et
63 al., 2009; Tomaz et al., 2018) and soot (Fan et al., 2020). During the haze episode, a



64 number of chemical processes occur in aqueous phase (Wong et al., 2017, 2019; Wu et
65 al., 2018b) and gas phase (Sumlin et al., 2017), which lead to significant changes in
66 chemical composition and light absorption properties of HULIS. For instance, recent
67 studies on oxidation of BB-derived BrC have indicated that although both enhancement
68 and bleaching of BrC occur during aging, bleaching of BrC becomes dominant over a
69 long period (Fan et al., 2020; Wong et al., 2017, 2019; Ni et al., 2021). However,
70 multiphase reaction between carbonyl and amine has demonstrated rapid formation of
71 light-absorbing organic compounds (Kampf et al., 2016). Nevertheless, it should be noted
72 that these results were mainly obtained from laboratory experiments and may not reflect
73 the complex evolution behavior of BrC in atmospheric environment.

74 High concentrations of HULIS have been determined during typical haze episodes
75 in northern, eastern, and southern China (Song et al., 2016; Win et al., 2020; Zhang et al.,
76 2020; Wang et al., 2020), and have been demonstrated to significantly influence
77 atmospheric visibility, environment, and photochemical process. Guangzhou is the
78 biggest city in the Pearl River Delta (PRD), one of the most developed regions in China,
79 and is located in the subtropical zone with a population of over 18 million people (Yu et
80 al., 2017). Although a remarkable decline in atmospheric particulate matter (PM_{2.5})
81 pollution has been observed in recent years owing to strict regulatory controls, O₃ and
82 VOCs still remain at higher levels and severe haze pollution caused by fine particulate
83 matter frequently occur in winter (Huang et al., 2014). Several studies have investigated
84 the chemical and optical properties of HULIS in the PRD region and found that both BB
85 and SOA formation have significant effects on these organic compounds in atmosphere
86 (Fan et al., 2016; Zhang et al., 2021; Jiang et al., 2020, 2021). However, detailed



87 information regarding the evolution of light absorption and molecular composition of
88 HULIS during haze events is still scarce.

89 Recently, ultrahigh-resolution Fourier transform ion cyclotron resonance mass
90 spectrometry (FT-ICR MS) coupled with electrospray ionization (ESI) sources has been
91 frequently employed to investigate the exact molecular characteristics of HULIS in
92 ambient aerosols (Tang et al., 2020; Song et al., 2018, 2022; Zeng et al., 2021). Owing to
93 its extremely high mass resolution and accuracy, this technique allows further exploration
94 of the evolution of HULIS during haze event. The present study performed
95 comprehensive characterization of HULIS in PM_{2.5} collected during a haze event in
96 Guangzhou, China. The abundances and light absorption properties of HULIS were first
97 measured, and carbonaceous fractions, water-soluble ions, and levoglucosan (Lev) were
98 determined. Subsequently, four HULIS samples collected during different haze stages
99 were analyzed using FT-ICR MS operated in both ESI⁻ and ESI⁺ modes. To our
100 knowledge, the present study is aim to apply a combination of optical properties and
101 molecular characterization by FT-ICR MS to investigate HULIS in a haze event in the
102 subtropical zone of China. The results obtained provide novel insights into the evolution
103 of HULIS during haze event, and are important for predicting the environmental and
104 climatic effects of HULIS in South China.

105 **2. Material and Methods**

106 **2.1. Aerosol sampling**

107 The PM_{2.5} samples were collected on the campus of Guangzhou Institute of
108 Geochemistry, Chinese Academy of Sciences, Guangzhou, China (23.14N, 113.35E),



109 which is an academic and residential region. Traffic emissions and residential activities
110 are the potential pollution sources in the sampling area. The 24-h PM_{2.5} sampling was
111 conducted using a high-volume sampler (Tianhong Intelligent Instrument Plant, Wuhan,
112 China, with a flow rate of 1.0 m³ min⁻¹) during 7 to 30 January of 2018, and a total of 24
113 samples were collected on the prebaked quartz filters (20.3 × 25.4 cm², Whatman,
114 Maidstone, UK). Field blank samples were collected without power on. After collection,
115 all filter samples were stored in a refrigerator at -20 °C until analysis. Meteorological
116 data (<http://www.wunderground.com/history/airport/ZGGG>), including wind speed,
117 temperature, relative humidity, and concentrations of SO₂, O₃, and NO₂, for the sampling
118 days are presented in Figure 1 and Table S1.

119 **2.2. Isolation of HULIS**

120 HULIS were isolated using a solid-phase extraction (SPE) procedure as described
121 previously (Zou et al., 2020). Briefly, portions of the PM_{2.5} samples (100 cm²) were
122 ultrasonically extracted with 50 mL of ultrapure water for 30 min. The extracts were
123 filtered through a 0.22-µm PTFE syringe filter and then adjusted to pH of 2 with HCl,
124 and loaded on a preconditioned SPE cartridge (Oasis HLB, 200 mg/6 mL, Waters, USA).
125 The hydrophilic fraction (i.e., inorganic ions, high-polar organic acids, etc) was removed
126 with ultrapure water, whereas the relatively hydrophobic HULIS fraction was retained
127 and eluted with 2% (v/v) ammonia/methanol. Finally, HULIS solution was evaporated to
128 dryness with a gentle N₂ stream and redissolved with ultrapure water for the analysis.

129 **2.3. Light absorption analysis**



130 The absorption spectra of the water-soluble organic carbon (WSOC) and HULIS
131 fractions were measured by a UV-vis spectrophotometer (UV-2600, Shimadzu) between
132 200 to 700 nm. Each spectrum was corrected for the filter blanks. The light absorption
133 coefficients, absorption Ångström exponent (AAE) and mass absorption efficiency
134 (MAE_{λ}) were calculated and the detailed methods are presented in the Supporting
135 Information (SI).

136 **2.4. FT-ICR MS analysis**

137 For FT-ICR MS analysis, the HULIS samples were isolated from $PM_{2.5}$ collected
138 during four periods: before haze days (clean-I days, 7–12 January), haze bloom days
139 (haze-I days, 13–18 January), haze decay days (haze-II days, 19–24 January), and after
140 haze days (clean-II days, 25–30 January). A filter punch (18 cm in diameter) was taken
141 from every sample, and all the six samples in each period was combined for the isolation
142 of HULIS fractions. The obtained HULIS samples were measured with an ESI FT-ICR
143 MS (Bruker Daltonik GmbH, Bremen, Germany) equipped with a 9.4 T refrigerated
144 actively shielded superconducting magnet. The system was operated in both ESI⁻ and
145 ESI⁺ modes. The scan range was set to m/z from 100 to 1000, with a typical mass-
146 resolving power $>450,000$ at m/z 319 with <0.2 ppm absolute mass error. The mass
147 spectra were calibrated externally with arginine clusters and internally recalibrated with
148 typical O_5 -class species peaks in DataAnalysis 4.4 (Bruker Daltonics). Due to the
149 inherent differences in the ionization mechanisms between ESI⁻ and ESI⁺ modes, the
150 data detected by the two ionization modes can provide complementary information on the
151 molecular composition of atmospheric HULIS (Lin et al., 2012; Lin et al., 2018). The
152 details of data analysis are provided in the SI.



153 **2.5. Chemical analysis**

154 The amounts of organic carbon (OC) and elemental carbon (EC) were determined by
155 a OC/EC analyzer (Sunset Laboratory Inc., USA) (Mo et al., 2018). The concentrations
156 of WSOC and HULIS were determined by a TOC analyzer (Shimadzu TOC_VCPH,
157 Kyoto, Japan). The water-soluble inorganic species (NO_3^- , SO_4^{2-} , Cl^- , NH_4^+ , K^+ , Na^+ ,
158 Ca^{2+} , Mg^{2+}) were measured with a Dionex ICS-900 ion chromatography system (Thermo
159 Fisher Scientific, USA) as described previously (Huang et al., 2018). The concentrations
160 of Lev were analyzed with a gas chromatography–MS after derivatization with BSTFA
161 and pyridine at 70 °C for 3 h (Huang et al., 2018). Detailed information regarding these
162 measurements is provided in the SI.

163 **3. Results and Discussion**

164 **3.1. Abundance and chemical composition of $\text{PM}_{2.5}$**

165 Figure 1 shows the meteorological conditions, $\text{PM}_{2.5}$ concentration, and
166 concentrations of major chemical constituents, including carbon fractions and water-
167 soluble inorganic ions in $\text{PM}_{2.5}$ samples obtained during a haze bloom-decay process.
168 Based on the variation in $\text{PM}_{2.5}$ concentration, these samples were categorized into four
169 groups: clean-I days (before haze, 14–24 $\mu\text{g m}^{-3}$), haze-I days (haze bloom, 45–114 μg
170 m^{-3}), haze-II days (haze decay, 58–115 $\mu\text{g m}^{-3}$), and clean-II days (after haze, 9–35 μg
171 m^{-3}). As indicated in Table S1 and Figure 1, the $\text{PM}_{2.5}$ concentrations increased from 18
172 $\pm 3.3 \mu\text{g m}^{-3}$ in clean-I days to 82 ± 26 and $84 \pm 22 \mu\text{g m}^{-3}$ in haze-I and haze-II days,
173 respectively, and then decreased to $21 \pm 10 \mu\text{g m}^{-3}$ in clean-II days. This finding
174 obviously indicated that the average $\text{PM}_{2.5}$ concentrations during the examined haze



175 episode are higher than the second-grade national ambient air quality standard in China
176 ($75 \mu\text{g m}^{-3}$, 24 h), whereas those during clean days are lower than the first-grade national
177 ambient air quality standard in China ($35 \mu\text{g m}^{-3}$, 24 h). However, the average $\text{PM}_{2.5}$
178 concentrations during the haze event are lower than those in the cities in winter haze,
179 including Shenyang ($108 \mu\text{g m}^{-3}$) (Zhang et al., 2020), and Nanjing ($123 \pm 28.5 \mu\text{g m}^{-3}$)
180 (Li et al., 2020), Beijing ($158 \mu\text{g m}^{-3}$), and Xi'an ($345 \mu\text{g m}^{-3}$) (Zhang et al., 2018). As
181 shown in Figure 1a, the wind speed decreased from 4 to 1.5 m s^{-1} during the haze bloom
182 process, resulting in stable meteorological conditions. Moreover, the $\text{PM}_{2.5}$ concentrations
183 were significantly negatively correlated with wind speed ($r = -0.77$; $p < 0.01$), indicating
184 that poor air dispersion condition leads to accumulation of particulate matter in the study
185 region.

186 As shown in Table S1, the average concentrations of OC and EC were 2.2–15 and
187 $0.36\text{--}2.7 \mu\text{gC m}^{-3}$ in the four stages, respectively, implying that the distinct changes in
188 OC and EC were higher during haze episodes than those in clear days. During the entire
189 study period, WSOC concentration ranged from 0.5 to $12.5 \mu\text{gC m}^{-3}$ ($4.3 \pm 1.2 \mu\text{gC m}^{-3}$),
190 which contributed to 53%–57% of OC in $\text{PM}_{2.5}$. The HULIS concentration noted in the
191 present study ranged from 0.15 to $6.1 \mu\text{gC m}^{-3}$ ($2.2 \pm 1.9 \mu\text{gC m}^{-3}$), which was
192 comparable to those observed in the PRD region, such as Hong Kong ($2.38 \pm 1.62 \mu\text{gC}$
193 m^{-3}) (Ma et al., 2019), Guangzhou ($2.4 \pm 1.6 \mu\text{gC m}^{-3}$) (Fan et al., 2016), and Heshan
194 ($2.08 \pm 1.16 \mu\text{gC m}^{-3}$) (Jiang et al., 2020), but lower than those in northern cities of
195 China, such as Xi'an ($12.4 \pm 6.5 \mu\text{gC m}^{-3}$) (Huang et al., 2020), Beijing (3.79 ± 3.03
196 $\mu\text{gC m}^{-3}$) (Mo et al., 2018), and Lanzhou ($4.7 \mu\text{gC m}^{-3}$) (Tan et al., 2016). As shown in
197 Figure 1, HULIS fraction also exhibited obvious variations during the entire sampling



198 period. The average HULIS concentration was $0.46 \pm 0.22 \mu\text{gC m}^{-3}$ in clean-I days,
199 which sharply increased to $4.5 \pm 1.2 \mu\text{gC m}^{-3}$ in haze-I days, then decreased to 3.1 ± 1.2
200 $\mu\text{gC m}^{-3}$ in haze-II days, and rapidly declined to $0.75 \pm 0.52 \mu\text{gC m}^{-3}$ in clean-II days.
201 This result was consistent with the changing trend of WSOC, OC, and EC. In addition,
202 the HULIS/WSOC ratios were about 0.50 ± 0.13 in the four $\text{PM}_{2.5}$ samples, which are in
203 broad agreement with other studies showing that HULIS is the major fraction of WSOC
204 (Fan et al., 2016; Ma et al., 2019; Jiang et al., 2020).

205 As illustrated in Figure 1, obvious variations in chemical compositions were also
206 observed in these $\text{PM}_{2.5}$ samples. Secondary inorganic aerosols (SIA) (i.e., SO_4^{2-} , NO_3^- ,
207 and NH_4^+), OC, and EC exhibited a similar variation during the entire study period, and
208 their contents sharply increased from 10 January in clean-I days to 13–18 January in
209 haze-I days, then slowly decreased in haze-II days, and finally reached lower levels in
210 clean-II days. It must be noted that the increasing rate of EC was similar to that of SIA in
211 haze-I days, indicating that direct emissions and atmospheric reactions may play similar
212 roles in $\text{PM}_{2.5}$ increase during this haze bloom period. As indicated in Figure 1f, the
213 highest values of $\text{NO}_3^-/\text{SO}_4^{2-}$ were observed in haze-I days, implying the important
214 influence of traffic exhausts in the haze bloom period (Mo et al., 2018). In addition, the
215 high NO_2 and O_3 concentrations and the stable meteorological condition with high
216 temperature also led to the outburst of fine particulate pollution in this period. During
217 haze-II days, the SIA and OM contents in $\text{PM}_{2.5}$ slowly decreased, whereas the
218 concentrations of Na^+ , Cl^- , and unidentified materials as well as the Lev/OC ratio in
219 $\text{PM}_{2.5}$ increased (Figure 1e,f,h), suggesting that local contribution weakened and regional
220 contribution via BB and sea salt became more important (Jiang et al., 2021). This



221 phenomenon was also observed to be consistent with the changes in the pollutant sources
222 transported by air masses. As indicated in Figure S1, the $PM_{2.5}$ samples in haze-II days
223 included some contributors transported from coastal area of eastern Guangdong Province
224 and Fujian Province, and the $PM_{2.5}$ particulates are likely to be enriched with sea salt
225 materials and mineral dusts.

226 3.2. Light absorption

227 The light absorption properties of WSOC and HULIS (Figure 1d, i, j and Table S2)
228 exhibited obvious temporal variations during the sampling period. The AAE values of
229 WSOC and HULIS ranged from 4.1 to 6.4 and 5.6 to 6.6, respectively. The AAE values
230 for HULIS were obviously higher than those for WSOC in the same sample (Figure 1i),
231 indicating that light absorption of HULIS is more wavelength-dependent than that of
232 WSOC. This difference may be related with the higher enrichment of light-absorbing
233 organic species in HULIS. Moreover, the AAE values of HULIS did not present
234 significant variation during the entire haze process.

235 Light absorption at 365 nm (Abs_{365}) for WSOC and HULIS were 2.5 ± 2.0 and $1.8 \pm$
236 1.6 M m^{-1} , respectively (Table S2). HULIS contributed to about 72% of light absorption
237 coefficients by WSOC, implying that they enriched the major light-absorbing
238 components in WSOC. As shown in Figure 1d, the Abs_{365} values for HULIS presented
239 obvious temporal variations. The $Abs_{365,HULIS}$ value was $0.55 \pm 0.06 \text{ M m}^{-1}$ in clean-I
240 days, which first increased to $3.4 \pm 1.5 \text{ M m}^{-1}$ in haze-I days and then slowly decreased to
241 $2.6 \pm 0.85 \text{ M m}^{-1}$ in haze-II days, and finally rapidly declined to $0.64 \pm 0.32 \text{ M m}^{-1}$ in
242 clean-II days. This result was similar to the variations in the mass concentration of
243 HULIS. Furthermore, the Abs_{365} values for HULIS in Guangzhou were found to be



244 higher than those observed in southeastern Tibetan Plateau ($0.38\text{--}1.0\text{ M m}^{-1}$) (Zhu et al.,
245 2018), but obviously lower than those in Xi'an ($7.6\text{--}36\text{ M m}^{-1}$) (Shen et al., 2017) and
246 Beijing, ($3.7\text{--}10.1\text{ M m}^{-1}$) (Du et al., 2014).

247 In general, MAE_{365} value can be used to assess the light absorption capacity of target
248 organic compounds (Li et al., 2019). As shown in Figure 1j and Table S2, the MAE_{365}
249 values for WSOC and HULIS were in the range of $0.68\text{--}1.3\text{ m}^2\text{ gC}^{-1}$ ($1.0 \pm 0.21\text{ m}^2\text{ gC}^{-1}$)
250 and $0.77\text{--}1.8\text{ m}^2\text{ gC}^{-1}$ ($1.1 \pm 0.27\text{ m}^2\text{ gC}^{-1}$), respectively, during the entire sampling period.
251 The generally higher MAE_{365} values for HULIS, when compared with those for WSOC
252 demonstrated that HULIS are enriched with strong light-absorbing compounds. Moreover,
253 the MAE_{365} values for HULIS measured in the present study were noted to be
254 comparable to those determined in Beijing ($1.43 \pm 0.33\text{ m}^2\text{ g C}^{-1}$) (Mo et al., 2018),
255 Xi'an ($0.91\text{--}1.85\text{ m}^2\text{ g C}^{-1}$) (Yuan et al., 2021), and Hong Kong ($1.84 \pm 0.77\text{ m}^2\text{ gC}^{-1}$)
256 (Ma et al., 2019). The average MAE_{365} values for HULIS exhibited some temporal
257 variations. The MAE_{365} values for HULIS were 0.91 ± 0.03 and $0.95 \pm 0.11\text{ m}^2\text{ gC}^{-1}$ in
258 haze-I and haze-II days, respectively, which were much lower than those (1.3 ± 0.22 and
259 $1.3 \pm 0.27\text{ m}^2\text{ gC}^{-1}$, respectively) observed in clean-I and clean-II days, suggesting that
260 HULIS have a relatively weaker light absorption capability in haze days. This finding is
261 consistent with the results reported by Zhang et al. (2017), who found that the MAE_{365}
262 values in the heating or non-heating seasons during hazy days were lower than those in
263 clean days. These differences in MAE_{365} values may potentially contribute to the stagnant
264 conditions prolonging secondary oxidation reaction or photolytic aging period, which
265 help the chromophores containing C=C unsaturated bond to be severely oxidized (Wang
266 et al., 2017a; Zhang et al., 2017). This process of reducing light absorption is also known



267 as "photobleaching" or photolytic aging, which often occurs in the aging process
268 (Forrister et al., 2015; Wong et al., 2017). Besides, an increase in additional sources for
269 HULIS in the study area, such as weaker or non-light-absorbing compounds formed by
270 atmospheric oxidation, could also result in weaker light absorption of HULIS during the
271 haze episode (Liu et al., 2018).

272 **3.3. Molecular evolution of HULIS during the haze process**

273 For an in-depth understanding of the variation in HULIS at molecular level during
274 the haze process, the four HULIS samples collected in different stages of the haze
275 process were analyzed by ESI FT-ICR MS in both negative and positive modes. As
276 shown in Figure 2, thousands of peaks were detected in the mass range between m/z 100
277 and m/z 700, with the high intensity ions noted within m/z 150–400 (Figure 2), which are
278 comparable to those of ambient HULIS determined in previous studies (Song et al., 2018,
279 2019, 2022; Wang et al., 2017b; Mo et al., 2018). As shown in Figure 2, some organic
280 compounds with stronger arbitrary abundance were labeled, and their formulas, double
281 bond equivalent (DBE), modified aromaticity index (AI_{mod}), and potential sources were
282 listed in Table S3. Compounds a ($C_7H_7NO_3$) and b ($C_8H_6O_4$), both have high DBE values,
283 which might be assigned to aromatics such as methylnitrophenol and phthalic acid.,
284 whereas compound d ($C_8H_{18}O_4S$) with low DBE value and high O/S ratio was probably
285 aliphatic organosulfate. These results suggested that both BB and vehicular emissions are
286 important sources of BrC in ambient aerosols (Mohr et al., 2013; Riva et al., 2015; Lin et
287 al., 2012). Furthermore, compound e ($C_{10}H_{17}NO_7S$) and compound f ($C_{10}H_{18}N_2O_{11}S$) in
288 Table S3 were found to be identical to the oxidation products of monoterpenes, suggest
289 that biogenic sources could contribute to the formation of HULIS (Surratt et al., 2008;



290 Wang et al., 2019b). Thus, HULIS could be affected by multiple sources during the haze
291 process, possibly including BB, biogenic sources, and anthropogenic emissions.

292 The identified formulas could be divided into seven compound categories, namely,
293 CHO⁻, CHON⁻, CHOS⁻, and CHONS⁻ detected in ESI⁻ mode and CHO⁺, CHN⁺, and
294 CHON⁺ detected in ESI⁺ mode. As illustrated in Figure 2, the CHO compounds were the
295 most abundant group in all the HULIS, accounting for 43%–50% and 51%–57% of the
296 overall compounds detected in the ESI⁻ and ESI⁺ modes, respectively. It must be noted
297 that relatively lower contents of CHO⁻ were detected during the haze episode (haze-I and
298 haze-II days) and CHO⁺ molecules in haze-I HULIS. The CHON compounds were the
299 second most abundant group in all the HULIS. As shown in Figure 2, the relative content
300 of CHON⁻ was 23% in clean-I days, which slightly increased to 24%–25% in haze
301 episode, and then decreased to 23% in clean-II days. In contrast, the relative content of
302 CHON⁺ compounds was 41% in clean-I days, which increased to 45% in haze-I days,
303 then fell to 42% in haze-II days and 41% in clean-II days. Both CHOS⁻ and CHONS⁻
304 compounds were identified in all the four HULIS, accounting for 19%–22% and 8%–11%
305 of the total identified compounds, respectively. The CHN⁺ compounds were the least
306 abundant (1.3%–3.6%) in the four HULIS samples, and were relatively higher during the
307 haze episode, especially in haze-I days.

308 Tables S4 and S5 show the relative abundance weighted elemental ratios, molecular
309 weight (MW), DBE, AI_{mod} , and carbon oxidation state (OS_C) for the identified
310 compounds in HULIS. The MW_w values for HULIS determined in the ESI⁻ mode in
311 haze-I and haze-II days were 302 and 283, respectively, which were higher than those in
312 clean-I and clean-II days (266 and 264, respectively). Similar variation was also observed



313 for MW_w for HULIS detected in ESI+ mode (Table S5). These results clearly indicated
314 that higher MW compounds constituted HULIS obtained during the haze episode. It has
315 been reported that high MW BrC compounds have relatively higher chemical resistance
316 and are the long-lived components in atmospheric aerosols (Dasari et al., 2019; Wong et
317 al., 2017). Therefore, HULIS compounds may undergo longer aging and higher oxidation
318 during haze episode, and are thereby characterized by relatively high MW values.

319 Furthermore, the molecular properties of HULIS in different stages of haze process
320 also exhibited some observable differences. As shown in Table S4, the HULIS samples in
321 haze episode detected by ESI- mode presented relatively lower $AI_{mod,w}$ values and
322 relatively higher O/C_w , O/N_w , and O/S_w ratios than those in clean days, indicating that
323 haze HULIS exhibited relatively lower aromaticity and higher oxidation degree than
324 clean HULIS. These differences can be attributed to bleaching or degradation of aromatic
325 compounds (i.e., nitroaromatic compounds or polycyclic aromatic hydrocarbons (PAHs))
326 by photooxidation during the haze process. In addition, increased contribution from
327 traffic emission and secondary reactions of bio-VOCs also decreased the aromaticity and
328 increased the oxidation degree of HULIS (Liu et al., 2016; Tang et al., 2020). These
329 changes in HULIS compounds led to the decrease in their MAE_{365} values during the haze
330 episode, as described above (Zhong and Jang, 2014; Song et al., 2019).

331 **3.3.1. CHO Compounds**

332 The CHO compounds bear O-containing functional groups, and have been
333 frequently detected in ambient aerosols. As shown in Figure 2, the CHO compounds were
334 the predominant component in the four HULIS samples, and the MW_w values for CHO-
335 and CHO+ compounds were 247–288 and 236–272, respectively, with relatively higher



336 MW_w values observed for the CHO group (CHO⁻ and CHO⁺) in haze HULIS, especially
337 in haze-I samples. This finding is comparable to that reported in a previous study in
338 which aqueous oxidation of BB mixtures was found to yield high MW of organic
339 products (Tomaz et al., 2018; Yu et al., 2016).

340 The OS_C is often used to describe the degree of oxidation of organic species in the
341 atmosphere (Kroll et al., 2011; Tong et al., 2019; Kourtchev et al., 2016). Figure 3 shows
342 plots of OS_C versus carbon number for the CHO compounds. As indicated in the figure,
343 CHO compounds exhibited OS_C from -2 to $+1$ with up to 40 carbon atoms. Kroll et al.
344 (2011) proposed that compounds with OS_C between -0.5 and $+1$ and < 18 carbon atoms
345 can be attributed to semi-volatile and low-volatile oxidized organic aerosols (SV-OOA
346 and LV-OOA), which are mainly formed by complex oxidation reactions in atmosphere.
347 Compounds with OS_C between -0.5 and -1.5 and 6–23 carbon atoms are related to
348 primary biomass burning organic aerosol (BBOA). In addition, compounds with OS_C
349 between -1 and -2 and ≥ 18 carbon atoms have been suggested to be hydrocarbon-like
350 organic aerosols (HOA), which are regarded as primary combustion surrogate (Zhang et
351 al., 2005; Kroll et al., 2011; Wang et al., 2017b).

352 As illustrated in Figure 3 and Table S6, most of the CHO⁻ compounds clustered in
353 the BBOA region, accounting for 40%–46% of the total CHO⁻ compounds, thus
354 suggesting that BB may be a major contributor to CHO compounds in HULIS. Figure 3
355 clearly indicates that the majority of aromatic and condensed aromatic compounds
356 produced signals in the OS_C region between -0.5 and 1.0 and carbon number of 3–18
357 (Figure 3), which corresponded to SV-OOA and LV-OOA. The proportions of SV-OOA
358 and LV-OOA accounted for 23%–28% and 1.9%–2.4% of the total CHO⁻ compounds,



359 respectively, and presented no significant variation. In contrast, the HOA components in
360 haze-I days showed the highest abundance (18%), which were much higher than those
361 (3.5%–4.5%) in haze-II, clean-I, and clean-II days. This finding indicated that the
362 increase in the primary source is associated with fossil fuel combustion such as vehicle
363 emissions during the haze bloom period (Zhang et al., 2005).

364 As shown in Figure 3, CHO⁺ compounds presented lower OS_C (from –2.0 to 1.0)
365 than CHO[–] compounds. Most of the CHO⁺ compounds occurred in the BBOA region in
366 all four HULIS samples, making up to 60%–72% of the total CHO⁺ compounds, which
367 were much higher than those detected in ESI[–] mode, indicating that primary organic
368 compounds produced from BB were preferably detected in ESI⁺ mode. The HOA among
369 CHO⁺ compounds showed the same changing trends as those among CHO[–] compounds,
370 and higher HOA abundance was observed during haze-I days. In addition, some high
371 AI_{mod} values of aromatics were found in the regions A1⁺ and A2⁺ (Figure 3), which
372 implied that the highest AI_{mod} values (AI ≥ 0.67) with DBE ≥ 22 were only detected
373 during the haze days possibly owing to soot-derived materials or oxidized PAHs
374 (Decesari et al., 2002; Kuang and Shang, 2020). It must be noted that the sampling site in
375 the present study is influenced by traffic sources, causing increased accumulation of
376 vehicle-exhausted soot during haze episode, which was confirmed by relatively low
377 BBOA content in haze-I days. Oxidation of soot particles could result in the formation of
378 water-soluble high aromatic organic species (Decesari et al., 2002).

379 3.3.2. CHON Compounds

380 In the present study, 1379–2217 and 2008–2943 formulas were assigned to CHON
381 compounds identified in the ESI[–] and ESI⁺ spectra, respectively, which accounted for



382 23%–25% (ESI⁻) and 41%–45% (ESI⁺) of total identified compounds, respectively.
383 Relatively higher contents of CHON⁻ compounds were obviously detected in HULIS
384 samples obtained during haze-I days, suggesting the occurrence of more N-containing
385 components in HULIS during haze bloom days. As shown in Tables S4 and S5, the
386 average MW_w values for CHON⁻ and CHON⁺ compounds were 328 and 317 in haze-I
387 days, respectively, which were slightly higher than those determined in haze-II days and
388 all higher than those observed in clean-I and clean-II days. Meanwhile, the AI_{mod,w} values
389 for CHON⁻ in haze days were 0.31–0.34, which were slightly lower than those in clean
390 days (0.37 and 0.40). These findings indicated that more high MW CHON compounds
391 with lower aromatic structures were formed during the haze episode.

392 The O/N_w ratios for CHON⁻ and CHON⁺ during haze-I and haze-II days were 5.3–
393 5.7 and 3.8, respectively, which were higher than those determined during the two clean
394 periods, confirming that these compounds were highly oxidized during the haze episode
395 (Tables S4 and S5). In general, compounds with O/N ≥ 3 may indicate oxidized N groups
396 such as nitro (–NO₂) or nitrooxy (–ONO₂), whereas compounds with O/N < 3 may denote
397 the reduced N compounds (i.e., amines) (Lin et al., 2012; Song et al., 2018). In the
398 present study, most of the CHON compounds (79%–91% of CHON⁻ compounds and
399 61%–64% of CHON⁺ compounds) exhibited O/N ≥ 3, suggesting that high
400 concentrations of nitro compounds or organonitrates were contained in the CHON
401 compounds. Moreover, these compounds were more abundant in the CHON⁻ group
402 during the haze episode (87%–91%), when compared with those during clean-I and
403 clean-II days (79%–82%), again implying that CHON⁻ compounds undergo relatively
404 higher oxidization during the haze episode. As indicated in Figure 1, the increase in NO₂



405 was consistent with increased production of highly oxidized N-containing organic
406 compounds (NOCs) during the haze episode, which suggested the significant contribution
407 of NO₃-related multigenerational chemistry to organonitrate aerosol formation
408 (Berkemeier et al., 2016).

409 The majority of aromatics and condensed aromatics produced clear signals in
410 regions associated with SV-OOA and LV-OOA (Figure 4). BBOA also constituted a
411 significant proportion (33%–39%) in the CHON– group, and a relatively lower BBOA
412 content was observed in haze-I days. The abundance of HOA was relatively lower,
413 accounting for 2.3%–7.8% of the total CHON compounds, and the relative abundance of
414 HOA in haze-I days was much higher than that in haze-II, clean-I, and clean-II days,
415 suggesting the accumulation of primary fossil fuel combustion during haze-I days.

416 The CHON+ compounds mainly occurred at the range of $-2.0 < OS_C < 1.5$, with
417 average OS_C values of around -1.0 for each sample, clearly indicating that CHON+
418 compounds were relatively lower than CHON– compounds. Most of the CHON+
419 compounds were detected in the BBOA region, accounting for 60%–76% of the total
420 CHON⁺ compounds. The relative contribution of BBOA in haze-I days was lower than
421 that in haze-II and clean days. Moreover, a large number of aromatic species were
422 observed at the region B1+ (Figure 4), demonstrating that higher aromatic compounds
423 were only detected in haze-I days, which may be related to soot or BC. Similar trend was
424 also exhibited by CHO+ compounds, indicating the important role of local combustion
425 sources (e.g., traffic emission) during haze-I days.

426

427



428 3.3.3. CHOS and CHONS Compounds

429 In this study, 478–696 CHOS compounds and 306–589 CHONS compounds were
430 identified in ESI– mode (Table S4). Among these S-containing compounds, >86% of the
431 CHOS compounds had O/S ratios >4, whereas > 89% of the CHONS compounds
432 presented O/S ratios >7, suggesting that these S-containing compounds were possibly
433 organosulfates and nitrooxyorganosulfates. As listed in Table S4, the $AI_{\text{mod,w}}$ values for
434 CHOS and CHONS were about 0.02 and 0.01 in the HULIS fraction, which were much
435 lower than those for CHO and CHON. Almost 99% of the CHOS and CHONS
436 compounds in the HULIS fraction had AI_{mod} values <0.5, while >93% of the CHONS
437 compounds had $AI_{\text{mod}} = 0$, indicating that they were mainly comprised of aliphatic and
438 olefinic organosulfates. These results are consistent with the previous findings that the
439 major S-containing compounds among organic aerosols in Guangzhou are organosulfates
440 formed by secondary oxidation reaction of long-chain alkenes/fatty acids with SO_2 (Jiang
441 et al., 2020), which generally possessed long aliphatic carbon chains and a higher degree
442 of oxidation. However, these compounds are different from the S-containing compounds
443 detected during the hazy days in Beijing (Jiang et al., 2016; Mo et al., 2016), which were
444 determined to be aliphatic organosulfates with low degree of oxidation and higher
445 amounts of aromatics and PAH-derived organosulfates, having a strong correlation with
446 anthropogenic emissions.

447 As described earlier, CHOS– and CHONS– compounds might be related to
448 organosulfates or nitrooxyorganosulfates, which have been observed to be derived from
449 atmospheric reactions of bio-VOCs such as α -pinene, limonene, and isoprene (Huang et
450 al., 2018; Surratt *et al.*, 2008) and fossil fuel combustion including coal combustion, off-



451 road engine emissions (Song et al., 2018, 2019; Cui et al., 2019). In the present study, the
452 relative contents of S-containing compounds (CHOS+CHONS) in the HULIS fraction in
453 haze days were all higher than those in clean days (Figure 2). Moreover, the CHOS and
454 CHONS compounds in haze HULIS always have relatively high relatively O/S ratios
455 than those in clean HULIS. These findings suggested the relatively higher contribution of
456 SO₂-related chemical oxidation during the haze event.

457 **3.3.4. CHN Compounds**

458 The N-bases (CHN) are usually identified in ambient aerosols and smokes from BB.
459 In the present study, 110–165 CHN⁺ compounds were identified in ESI⁺ mode, with
460 most of them (>86%) presenting DBE \geq 2, suggesting that they might be nitrile and
461 amine species (Lin et al., 2012). As shown in Figure 2, the abundances of CHN⁺
462 compounds were 2.0%–3.6% in the haze days, which were much higher than those noted
463 in clean days (1.3%–1.4%), indicating higher contribution of CHN⁺ compounds to the
464 HULIS fraction during the haze episode. The MW_w values for CHN⁺ compounds were
465 204–223, which were lower than those for the other groups (i.e., CHO⁺, CHON⁺) (Table
466 S5). However, the average AI_{mod} values for N-bases (0.37–0.48) detected in the ESI⁺
467 mode were much higher than those for CHO⁺ (0.11–0.12) and CHON⁺ (0.20–0.22)
468 compounds, implying that these reduced CHN⁺ compounds exhibited more unsaturated
469 or aromatic structures.

470 To further understand the molecular distribution of CHN⁺ compounds during the
471 haze process, van Krevelen (VK) diagrams were constructed by plotting the H/C ratio
472 versus N/C ratio (Figure S2). It was obvious that this plot could separate the compound
473 classes with different degree of AI. As shown in Figure S2, compounds (denoted in black



474 color) in the upper region of the VK diagram had one N atom with DBE = 0, indicating
475 that they are aliphatic amines. It can be noted from Table S7 that the aliphatic group
476 presented the lowest abundance in all the samples, suggesting that the CHN⁺ compounds
477 possessed comparatively lower aliphatic structures. Olefinic compounds showed the
478 highest abundance in the four samples, which accounted for 37%–51% of the total CHN⁺
479 compounds. Importantly, a large proportion of the compounds (>39%) exhibited high
480 degree of AI (AI > 0.5) (Figure S2 and Table S7), suggesting a large amounts of aromatic
481 structure and N-heterocyclic ring in HULIS. Moreover, the CHN⁺ compounds in haze-I
482 days presented obviously lower content of aromatic structures than those in haze-II,
483 clean-I, and clean-II days, signifying the relatively high contribution of fossil fuel
484 combustion (which generally emits more low-aromatic CHN compounds) during the haze
485 bloom episode(Song et al., 2022). In addition, the CHN⁺ group also constituted a large
486 proportion of BBOA (Table S6), which indicated the significant contribution of BB.
487 However, it must be noted that a relatively lower content of BBOA was detected during
488 haze-I days, which was consistent with the changing trends of CHON⁻ or CHON⁺
489 compounds during the haze episode. These results suggested the relatively lower
490 contribution of BB during haze-I days, because quiet and stable weather conditions can
491 prevent regional transport of BB sources during this stage (Wu et al., 2018b).

492 **3.4. Factors influencing light absorption and molecular characteristics of HULIS** 493 **during the haze bloom-decay process**

494 As described earlier, the light absorption properties of HULIS exhibited obvious
495 variation during the haze bloom-decay process. The average Abs₃₆₅ value for HULIS was
496 $0.55 \pm 0.06 \text{ M m}^{-1}$ in clean-I days, which first increased to $3.4 \pm 1.5 \text{ M m}^{-1}$ in haze-I days,



497 then slowly decreased to $2.6 \pm 0.85 \text{ M m}^{-1}$ in haze-II days, and finally rapidly declined to
498 $0.64 \pm 0.32 \text{ M m}^{-1}$ in clean-II days. In general, the light absorption of HULIS can be
499 related to their chemical and molecular properties that are influenced by factors such as
500 sources, secondary formation, and aging process. The results of principal component
501 analysis (PCA) obviously showed a positive loading for principal component 1 (PC1),
502 and the Abs_{365} values for HULIS were clustered with EC, K_{bb}^+ , Lev, NH_4^+ , and NO_3^-
503 (Figure 5). These results suggested that BB and other sources such as new particle
504 formation could contribute to light absorption of HULIS (Huang et al., 2014; An et al.,
505 2019; Song et al., 2019). Similarly, the findings of Pearson correlation coefficient
506 analysis revealed that the Abs_{365} values for HULIS exhibited significant positive
507 correlations with K_{bb}^+ ($r = 0.728$, $p < 0.01$) and Lev ($r = 0.800$, $p < 0.01$) (Table S8). As
508 Lev and K_{bb}^+ are generally considered as tracers derived from BB, these results suggested
509 the significant contribution of BB to light absorption of HULIS. This observation was
510 also supported by the abundance of BBOA compounds detected in all the four HULIS
511 samples (Table S6). The significant positive relationships between the Abs_{365} values for
512 HULIS and secondary ions (i.e., NO_3^- ($r = 0.702$, $p < 0.01$), SO_4^{2-} ($r = 0.554$, $p < 0.05$),
513 and NH_4^+ ($r = 0.899$, $p < 0.01$)) indicated the important impact of secondary formation on
514 the light absorption of HULIS. Besides, the Abs_{365} values for HULIS were also strongly
515 correlated with NO_2 , O_3 , and NO_2 , which confirmed the important impact of atmospheric
516 oxidation reactions on the light absorption of HULIS.

517 It must be noted that MAE_{365} is a key parameter signifying the light absorption
518 ability of HULIS. As listed in Table S2, the MAE_{365} values for HULIS varied in different
519 stages, and were lower in haze days owing to the variation in the chemical and molecular



520 composition of HULIS during the haze bloom-decay process. Furthermore, the AI_{mod}
521 values for HULIS varied in different stages (Tables S4 and S5), and were relatively lower
522 in haze days, indicating that haze HULIS have comparatively lower degree of
523 conjugation or aromaticity. This finding suggested that the HULIS compounds may
524 undergo higher oxidation and present longer aging period under specific quiet and stable
525 weather conditions during the haze episode, causing a decline in chromophores and
526 reduction in the light absorption capacity of HULIS (Lin et al., 2017). Besides, the
527 accumulated contribution of organic compounds from vehicle emission and secondary
528 chemical reactions of bio-VOCs may also dilute light-absorbing compounds in haze
529 HULIS (Tang et al., 2020; Liu et al., 2016).

530 Lin et al. (2018) reported that potential light-absorbing chromophores can be
531 determined in the region between $DBE = 0.5 \times C$ (linear conjugated polyenes $C_xH_yC_2$)
532 and $DBE = 0.9 \times C$ (fullerene-like hydrocarbons). In the present study, most of the high-
533 intensity CHON, CHO, and CHN compounds with high AI values were clustered in
534 potential BrC chromophore region (Figures S3 and S4), which mainly comprised CHON
535 (46%–50% in ESI- mode and 56%–62% in ESI+ mode, respectively) and CHO (44%–48%
536 in ESI- mode and 29%–38% in ESI+ mode, respectively) compounds (Table 1).
537 Although the contribution of CHN+ compounds to BrC was relatively lower, the content
538 of potential chromophores among the total CHN+ compounds was higher than those in
539 CHON+ and CHO+ compounds. Therefore, these three groups of light-absorbing
540 compounds (i.e., CHON+, CHN+, and CHO+ compounds) were further examined. As
541 shown in Table 1, the Int_C/Int_{BrC} values of CHO- (i.e., content of CHO- chromophores
542 in the total chromophores) decreased from 48% to 44% whereas the Int_C/Int_{BrC} values of



543 CHON⁻ increased from 46% to 50% during the haze bloom process. These findings
544 indicated that more NOCs chromophores were formed during this stage in which higher
545 NO₂ concentration may be preferred for the formation of N-containing chromophores
546 such as nitrophenols. However, it must be noted that the proportions of both CHO⁻ and
547 CHON⁻ chromophores among the total identified compounds decreased from clean-I to
548 haze-I days, suggesting the occurrence of stronger photo-bleaching process during the
549 haze bloom stage (Zeng et al., 2020). Likewise, both CHO⁺ and CHON⁺ compounds
550 presented similar variation during the entire study period. In addition, the CHN⁺
551 compounds also exhibited higher Int_C/Int_{B₁C} values during the haze bloom process and
552 suggesting the accumulated contribution from local combustion process. Furthermore, the
553 proportion of CHON⁺ chromophores in the total CHON⁺ compounds increased with the
554 decreasing content of CHN⁺ chromophores, may implying that some aromatic CHN⁺
555 compounds were transformed to CHON⁺ compounds during the aging process.

556

557 **4. Conclusions**

558 This study investigated the evolution of light absorption and molecular properties of
559 HULIS during a winter haze bloom-decay process, and examined the key factors
560 affecting the light absorption of HULIS in Guangzhou, China. The results showed that
561 HULIS exhibited significant variation in light absorption during the haze bloom-decay
562 process. First, higher Abs₃₆₅ values were observed in haze days, indicating the presence
563 of significant amounts of light-absorbing organic compounds during the haze episode.
564 However, the MAE₃₆₅ values for HULIS in haze days were relatively lower than those in
565 clean days, suggesting the light absorption capabilities of HULIS were weakened during



566 the haze event. Furthermore, CHON and CHO compounds, exhibiting relatively higher
567 degree of conjugated structure, were the most abundant groups in all the HULIS samples,
568 and were also the major contributors to light absorption capacity of HULIS. Importantly,
569 the molecular properties of HULIS dynamically varied during the entire haze episode.
570 When compared with HULIS in clean days, those in haze days presented relatively lower
571 AI_{mod} values and higher O/C_w , O/N_w , and O/S_w ratios, suggesting the predominance of
572 compounds with low aromaticity and higher oxidation in HULIS during haze episode.
573 These results indicated that HULIS compounds undergo relatively stronger oxidation and
574 longer aging process during the haze process. Moreover, PCA and Pearson correlation
575 analysis revealed that BB and secondary chemical formation both contributed to the
576 variation in the light absorption properties of HULIS. Both primary sources (such as
577 accumulated contribution of organic compounds formed from local traffic emission) and
578 secondary sources (such as stronger chemical reactions) led to the rapid increase in
579 HULIS during the haze bloom days. However, longer periods for oxidation and aging of
580 HULIS compounds were observed during the haze episode, and some potential BrC
581 chromophores were degraded. In addition, the chemical reactions of bio-VOCs such as
582 isoprene also diluted the light-absorbing compounds in HULIS.

583 Thus, the present study provides novel insights into the light and molecular
584 evolution of HULIS during haze event, which are important for predicting the
585 environmental and climatic effects of HULIS. However, as this study examined only one
586 haze bloom-decay process in winter in Guangzhou, the results obtained may be not
587 adequate for understanding all the haze episodes in South China. Therefore, there is a



588 need for a comprehensive investigation of haze episode in different seasons and regions
589 in future.

590

591 **Data availability**

592 The research data are available in the Harvard Dataverse
593 (<https://doi.org/10.7910/DVN/DYGYQT>, Song, 2022).

594

595 **Author contributions.** J. Song and P. Peng designed the research together. C. Zou, T.
596 Cao, and M. Li carried out the PM_{2.5} sampling experiments. C. Zou and T. Cao extracted
597 and analyzed the WSOC and HULIS samples. B. Jiang analyzed the HULIS samples by
598 FT-ICR MS. C. Zou and J. Song wrote the paper. J. Li, X. Ding, Z Yu, and G. Zhang
599 commented and revised the paper.

600

601 **Competing interests.** The authors declare that they have no conflict of interest

602

603 **Acknowledgments.** This study was supported by the National Natural Science
604 Foundation of China (42192514 and 41977188), Guangdong Foundation for Program of
605 Science and Technology Research (2020B1212060053), and Guangdong Foundation for
606 Program of Science and Technology Research (2019B121205006).

607

608 **References**

609 An, Z., Huang, R. J., Zhang, R., Tie, X., Li, G., Cao, J., Zhou, W., Shi, Z., Han, Y., Gu,
610 Z., and Ji, Y.: Severe haze in northern China: A synergy of anthropogenic emissions



- 611 and atmospheric processes, *Proc Natl Acad Sci U S A*, 116, 8657-8666,
612 10.1073/pnas.1900125116, 2019.
- 613 Berkemeier, T., Ammann, M., Mentel, T. F., Poschl, U., and Shiraiwa, M.: Organic
614 Nitrate Contribution to New Particle Formation and Growth in Secondary Organic
615 Aerosols from alpha-Pinene Ozonolysis, *Environ Sci Technol*, 50, 6334-6342,
616 10.1021/acs.est.6b00961, 2016.
- 617 Bianco, A., Deguillaume, L., Vaitilingom, M., Nicol, E., Baray, J. L., Chaumerliac, N.,
618 and Bridoux, M.: Molecular Characterization of Cloud Water Samples Collected at
619 the Puy de Dome (France) by Fourier Transform Ion Cyclotron Resonance Mass
620 Spectrometry, *Environ Sci Technol*, 52, 10275-10285, doi:10.1021/acs.est.8b01964,
621 2018.
- 622 Chen, Q., Wang, M., Wang, Y., Zhang, L., Li, Y., and Han, Y.: Oxidative Potential of
623 Water-Soluble Matter Associated with Chromophoric Substances in PM_{2.5} over
624 Xi'an, China, *Environ Sci Technol*, 53, 8574-8584, 10.1021/acs.est.9b01976, 2019.
- 625 Cui, M., Li, C., Chen, Y. J., Zhang, F., Li, J., Jiang, B., Mo, Y., Li, J., Yan, C., Zheng,
626 M., Xie, Z., Zhang, G., and Zheng, J.: Molecular characterization of polar organic
627 aerosol constituents in off-road engine emissions using Fourier transform ion
628 cyclotron resonance mass spectrometry (FT-ICR MS): implications for source
629 apportionment, *Atmos Chem Phys*, 19, 13945-13956, doi:10.5194/acp-19-13945-
630 2019, 2019.
- 631 Dasari, S., Andersson, A., Bikkina, S., Holmstrand, H., Budhavant, K., Satheesh, S.,
632 Asmi, E., Kesti, J., Backman, J., Salam, A., Bisht, D. S., Tiwari, S., Hameed, Z., and
633 Gustafsson, Ö.: Photochemical degradation affects the light absorption of water-



- 634 soluble brown carbon in the South Asian outflow, *Sci Adv*, 5, eaau8066, doi:
635 10.1126/sciadv.aau8066, 2019.
- 636 Decesari, S., Facchini, M. C., Matta, E., Mircea, M., Fuzzi, S., Chughtai, A. R., and
637 Smith, D. M.: Water soluble organic compounds formed by oxidation of soot, *Atmos*
638 *Environ*, 36, 1827-1832, 10.1016/s1352-2310(02)00141-3, 2002.
- 639 Du, Z., He, K., Cheng, Y., Duan, F., Ma, Y., Liu, J., Zhang, X., Zheng, M., and Weber,
640 R.: A yearlong study of water-soluble organic carbon in Beijing II: Light absorption
641 properties, *Atmos Environ*, 89, 235-241, 10.1016/j.atmosenv.2014.02.022, 2014.
- 642 Fan, X., Song, J., and Peng, P.: Temporal variations of the abundance and optical
643 properties of water soluble Humic-Like Substances (HULIS) in PM_{2.5} at Guangzhou,
644 China, *Atmos Res*, 172-173, 8-15, doi:10.1016/j.atmosres.2015.12.024, 2016.
- 645 Fan, X., Cao, T., Yu, X., Wang, Y., Xiao, X., Li, F., Xie, Y., Ji, W., Song, J., and Peng, P:
646 The evolutionary behavior of chromophoric brown carbon during ozone aging of fine
647 particles from biomass burning, *Atmos Chem Phys*, 20, 4593-4605, doi:10.5194/acp-
648 20-4593-2020, 2020.
- 649 Forrister, H., Liu, J., Scheuer, E., Dibb, J., Ziemba, L., Thornhill, K. L., Anderson, B.,
650 Diskin, G., Perring, A. E., Schwarz, J. P., Campuzano - Jost, P., Day, D. A., Palm, B.
651 B., Jimenez, J. L., Nenes, A., and Weber, R. J.: Evolution of brown carbon in
652 wildfire plumes, *Geophysical Research Letters*, 42, 4623-4630,
653 10.1002/2015gl063897, 2015.
- 654 Graber and Rudich: Atmospheric HULIS: How humic-like are they? A comprehensive
655 and critical review, *Atmos. Chem. Phys.*, 6, 729-753, 2006.



- 656 Huang, R. J., Yang, L., Cao, J., Chen, Y., Chen, Q., Chen, Q., Li, Y. J., Duan, J., Zhu, C.
657 C., Dai, W. T., Wang, K., Lin, C. S.; Ni, H. Y., Corbin, J. C., Wu, Y. F., Zhang, R. J.
658 Tie, X. X., Hoffmann, T., O'Dowd, C., and Dusek, U.: Brown Carbon Aerosol in
659 Urban Xi'an, Northwest China: The Composition and Light Absorption Properties,
660 *Environ Sci Technol*, 52, 6825-6833, doi:10.1021/acs.est.8b02386, 2018.
- 661 Huang, R. J., Zhang, Y., Bozzetti, C., Ho, K. F., Cao, J. J., Han, Y., Daellenbach, K. R.,
662 Slowik, J. G., Platt, S. M., Canonaco, F., Zotter, P., Wolf, R., Pieber, S. M., Bruns, E.
663 A., Crippa, M., Ciarelli, G., Piazzalunga, A., Schwikowski, M., Abbaszade, G.,
664 Schnelle-Kreis, J., Zimmermann, R., An, Z., Szidat, S., Baltensperger, U., El Haddad,
665 I., and Prevot, A. S.: High secondary aerosol contribution to particulate pollution
666 during haze events in China, *Nature*, 514, 218-222, 10.1038/nature13774, 2014.
- 667 Huang, R. J., Yang, L., Shen, J. C., Yuan, W., Gong, Y. Q., Guo, J., Cao, W., Duan, J.,
668 Ni, H., Zhu, C., Dai, W., Li, Y., Chen, Y., Chen, Q., Wu, Y., Zhang, R., Dusek, U.,
669 O'Dowd, C., and Hoffmann, T.: Water-Insoluble Organics Dominate Brown Carbon
670 in Wintertime Urban Aerosol of China: Chemical Characteristics and Optical
671 Properties, *Environ Sci Technol*, 54, 7836-7847, doi:10.1021/acs.est.0c01149, 2020.
- 672 Jiang, H., Li, J., Chen, D., Tang, J., Cheng, Z., Mo, Y., Su, T., Tian, C., Jiang, B., Liao,
673 Y., and Zhang, G.: Biomass burning organic aerosols significantly influence the light
674 absorption properties of polarity-dependent organic compounds in the Pearl River
675 Delta Region, China, *Environ Int*, 144, 106079, 10.1016/j.envint.2020.106079, 2020.
- 676 Jiang, H., Li, J., Sun, R., Liu, G., Tian, C., et al. Determining the Sources and
677 Transport of Brown Carbon Using Radionuclide Tracers and Modeling, *J*
678 *Geophys Res Atmos*, 126, e2021JD034616, doi:org/10.1029/2021JD034616, 2021.



- 679 Kampf, C. J., Filippi, A., Zuth, C., Hoffmann, T., and Opatz, T.: Secondary brown
680 carbon formation via the dicarbonyl imine pathway: nitrogen heterocycle formation
681 and synergistic effects, *Phys Chem Chem Phys*, 18, 18353-18364,
682 10.1039/c6cp03029g, 2016.
- 683 Kourtchev, I., Godoi, R. H. M., Connors, S., Levine, J. G., Archibald, A. T., Godoi, A. F.
684 L., Paralovo, S. L., Barbosa, C. G. G., Souza, R. A. F., Manzi, A. O., Seco, R.,
685 Sjostedt, S., Park, J.-H., Guenther, A., Kim, S., Smith, J., Martin, S. T., and Kalberer,
686 M.: Molecular composition of organic aerosols in central Amazonia: an ultra-high-
687 resolution mass spectrometry study, *Atmospheric Chemistry and Physics*, 16, 11899-
688 11913, 10.5194/acp-16-11899-2016, 2016.
- 689 Kroll, J. H., Donahue, N. M., Jimenez, J. L., Kessler, S. H., Canagaratna, M. R., Wilson,
690 K. R., Altieri, K. E., Mazzoleni, L. R., Wozniak, A. S., Bluhm, H., Mysak, E. R.,
691 Smith, J. D., Kolb, C. E., and Worsnop, D. R.: Carbon oxidation state as a metric for
692 describing the chemistry of atmospheric organic aerosol, *Nature Chemistry*, 3, 133-
693 139, 10.1038/nchem.948, 2011.
- 694 Kuang, K. and Shang, J.: Changes in light absorption by brown carbon in soot particles
695 due to heterogeneous ozone aging in a smog chamber, *Environ. Pollut.*, 266, 115273,
696 10.1016/j.envpol.2020.115273, 2020.
- 697 Laskin, A., Laskin, J., and Nizkorodov, S. A.: Chemistry of atmospheric brown carbon,
698 *Chem Rev*, 115, 4335-4382, 10.1021/cr5006167, 2015.
- 699 Li, M., Fan, X., Zhu, M., Zou, C., Song, J., Wei, S., Jia, W., and Peng, P.: Abundance
700 and light absorption properties of brown carbon emitted from residential coal



- 701 combustion in China, *Environ Sci Technol*, 53, 595-603,
702 doi:10.1021/acs.est.8b05630, 2019.
- 703 Li, S. W., Chang, M., Li, H., Cui, X. Y., and Ma, L. Q.: Chemical compositions and
704 source apportionment of PM_{2.5} during clear and hazy days: Seasonal changes and
705 impacts of Youth Olympic Games, *Chemosphere*, 256, 127163,
706 10.1016/j.chemosphere.2020.127163, 2020.
- 707 Lin, P., Bluvshstein, N., Rudich, Y., Nizkorodov, S. A., Laskin, J., and Laskin, A.:
708 Molecular chemistry of atmospheric brown carbon inferred from a nationwide
709 biomass burning event, *Environ Sci Technol*, 51, 11561-11570,
710 10.1021/acs.est.7b02276, 2017.
- 711 Lin, P., Rincon, A. G., Kalberer, M., and Yu, J. Z.: Elemental composition of HULIS in
712 the Pearl River Delta Region, China: results inferred from positive and negative
713 electrospray high resolution mass spectrometric data, *Environ Sci Technol*, 46, 7454-
714 7462, 10.1021/es300285d, 2012.
- 715 Lin, P., Fleming, L. T., Nizkorodov, S. A., Laskin, J., and Laskin, A.: Comprehensive
716 Molecular Characterization of Atmospheric Brown Carbon by High Resolution Mass
717 Spectrometry with Electrospray and Atmospheric Pressure Photoionization, *Anal*
718 *Chem*, 90, 12493-12502. doi:10.1021/acs.analchem.8b02177, 2018.
- 719 Liu, J., Lin, P., Laskin, A., Laskin, J., Kathmann, S. M., Wise, M., Caylor, R., Imholt, F.,
720 Selimovic, V., and Shilling, J. E.: Optical properties and aging of light-absorbing
721 secondary organic aerosol, *Atmospheric Chemistry and Physics*, 16, 12815-12827,
722 10.5194/acp-16-12815-2016, 2016.



- 723 Liu, J., Mo, Y., Ding, P., Li, J., Shen, C., and Zhang, G.: Dual carbon isotopes (^{14}C
724 and ^{13}C) and optical properties of WSOC and HULIS-C during winter in
725 Guangzhou, China, *Sci Total Environ*, 633, 1571-1578,
726 10.1016/j.scitotenv.2018.03.293, 2018.
- 727 Ma, Y., Cheng, Y., Qiu, X., Cao, G., Kuang, B., Yu, J. Z., and Hu, D.: Optical properties,
728 source apportionment and redox activity of humic-like substances (HULIS) in
729 airborne fine particulates in Hong Kong, *Environ Pollut*, 255, 113087,
730 10.1016/j.envpol.2019.113087, 2019.
- 731 Mo, Y., Li, J., Jiang, B., Su, T., Geng, X., Liu, J., Jiang, H., Shen, C., Ding, P., Zhong, G.,
732 Cheng, Z., Liao, Y., Tian, C., Chen, Y., and Zhang, G.: Sources, compositions, and
733 optical properties of humic-like substances in Beijing during the 2014 APEC summit:
734 Results from dual carbon isotope and Fourier-transform ion cyclotron resonance
735 mass spectrometry analyses, *Environ Pollut*, 239, 322-331,
736 10.1016/j.envpol.2018.04.041, 2018.
- 737 Mohr, C., Lopez-Hilfiker, F. D., Zotter, P., Prevot, A. S., Xu, L., Ng, N. L., Herndon, S.
738 C., Williams, L. R., Franklin, J. P., Zahniser, M. S., Worsnop, D. R., Knighton, W.
739 B., Aiken, A. C., Gorkowski, K. J., Dubey, M. K., Allan, J. D., and Thornton, J. A.:
740 Contribution of nitrated phenols to wood burning brown carbon light absorption in
741 Detling, United Kingdom during winter time, *Environ Sci Technol*, 47, 6316-6324,
742 10.1021/es400683v, 2013.
- 743 Ni, H., Huang, R. J., Pieber, S. M., Corbin, J. C., Stefenelli, G., Pospisilova, V., Klein, F.,
744 Gysel-Beer, M., Yang, L., Baltensperger, U., Haddad, I. E., Slowik, J. G., Cao, J.,
745 Prevot, A. S. H., and Dusek, U.: Brown Carbon in Primary and Aged Coal



- 746 Combustion Emission, Environ Sci Technol, 55, 5701-5710,
747 10.1021/acs.est.0c08084, 2021.
- 748 Park, S., Yu, G.-H., and Lee, S.: Optical absorption characteristics of brown carbon
749 aerosols during the KORUS-AQ campaign at an urban site, Atmospheric Research,
750 203, 16-27, 10.1016/j.atmosres.2017.12.002, 2018.
- 751 Rincón, A. G., Guzmán, M. I., Hoffmann, M. R., and Colussi, A. J.: Thermochromism of
752 Model Organic Aerosol Matter, The Journal of Physical Chemistry Letters, 1, 368-
753 373, 10.1021/jz900186e, 2009.
- 754 Shen, Z., Zhang, Q., Cao, J., Zhang, L., Lei, Y., Huang, Y., Huang, R. J., Gao, J., Zhao,
755 Z., Zhu, C., Yin, X., Zheng, C., Xu, H., and Liu, S.: Optical properties and possible
756 sources of brown carbon in PM 2.5 over Xi'an, China, Atmospheric Environment,
757 150, 322-330, 10.1016/j.atmosenv.2016.11.024, 2017.
- 758 Simoneit, B. R. T., Rushdi, A. I., Bin Abas, M. R., and Didyk, B. M.: Alkyl amides and
759 nitriles as novel tracers for biomass burning, Environmental Science & Technology,
760 37, 16-21, 10.1021/es020811y, 2003.
- 761 Song, J.: Data for SJ, Harvard Dataverse [data set],
762 (<https://doi.org/10.7910/DVN/DYGYQT>), 2022.
- 763 Song, J. Z., Li, M. J., Fan, X. J., Zou, C. L., Zhu, M. B., Jiang, B., Yu, Z. Q., Jia, W. L.,
764 Liao, Y. H., and Peng, P. A.: Molecular Characterization of Water- and Methanol-
765 Soluble Organic Compounds Emitted from Residential Coal Combustion Using
766 Ultrahigh-Resolution Electrospray Ionization Fourier Transform Ion Cyclotron
767 Resonance Mass Spectrometry, Environ Sci Technol, 53, 13607-13617,
768 10.1021/acs.est.9b04331, 2019.



- 769 Song, J. Z., Li, M. J., Jiang, B., Wei, S. Y., Fan, X. J., and Peng, P. A.: Molecular
770 Characterization of Water-Soluble Humic like Substances in Smoke Particles
771 Emitted from Combustion of Biomass Materials and Coal Using Ultrahigh-
772 Resolution Electrospray Ionization Fourier Transform Ion Cyclotron Resonance
773 Mass Spectrometry, *Environ Sci Technol*, 52, 2575-2585, 10.1021/acs.est.7b06126,
774 2018.
- 775 Song, J. Z., Li, M. J., Zou, C. L., Cao, T., Fan, X. J., Jiang, B., Yu, Z. Q., Jia, W. L., and
776 Peng, P. A.: Molecular Characterization of Nitrogen-Containing Compounds in
777 Humic-like Substances Emitted from Biomass Burning and Coal Combustion,
778 *Environ Sci Technol*, 56, 119-130, doi:10.1021/acs.est.1c04451, 2022.
- 779 Sumlin, B. J., Pandey, A., Walker, M. J., Pattison, R. S., Williams, B. J., and Chakrabarty,
780 R. K.: Atmospheric Photooxidation Diminishes Light Absorption by Primary Brown
781 Carbon Aerosol from Biomass Burning, *Environ Sci Tech Lett*, 4, 540-545,
782 10.1021/acs.estlett.7b00393, 2017.
- 783 Surratt, J. D., Gomez-Gonzalez, Y., Chan, A. W. H., Vermeylen, R., Shahgholi, M.,
784 Kleindienst, T. E., Edney, E. O., Offenberg, J. H., Lewandowski, M., Jaoui, M.,
785 Maenhaut, W., Claeys, M., Flagan, R. C., and Seinfeld, J. H.: Organosulfate
786 formation in biogenic secondary organic aerosol, *J Phys Chem A*, 112, 8345-8378,
787 10.1021/jp802310p, 2008.
- 788 Tan, J., Xiang, P., Zhou, X., Duan, J., Ma, Y., He, K., Cheng, Y., Yu, J., and Querol, X.:
789 Chemical characterization of humic-like substances (HULIS) in PM_{2.5} in Lanzhou,
790 China, *Sci Total Environ*, 573, 1481-1490, 10.1016/j.scitotenv.2016.08.025, 2016.



- 791 Tang, J., Li, J., Su, T., Han, Y., Mo, Y. Z., Jiang, H. X., Cui, M., Jiang, B., Chen, Y. J.,
792 Tang, J. H., Song, J. Z., Peng, P. A., and Zhang, G.: Molecular compositions and
793 optical properties of dissolved brown carbon in biomass burning, coal combustion,
794 and vehicle emission aerosols illuminated by excitation-emission matrix
795 spectroscopy and Fourier transform ion cyclotron resonance mass spectrometry
796 analysis, *Atmos Chem Phys*, 20, 2513-2532, 10.5194/acp-20-2513-2020, 2020.
- 797 Tomaz, S., Cui, T., Chen, Y., Sexton, K. G., Roberts, J. M., Warneke, C., Yokelson, R. J.,
798 Surratt, J. D., and Turpin, B. J.: Photochemical Cloud Processing of Primary
799 Wildfire Emissions as a Potential Source of Secondary Organic Aerosol, *Environ Sci*
800 *Technol*, 52, 11027-11037, 10.1021/acs.est.8b03293, 2018.
- 801 Tong, H., Zhang, Y., Filippi, A., Wang, T., Li, C., Liu, F., Leppla, D., Kourtchev, I.,
802 Wang, K., Keskinen, H. M., Levula, J. T., Arangio, A. M., Shen, F., Ditas, F., Martin,
803 S. T., Artaxo, P., Godoi, R. H. M., Yamamoto, C. I., de Souza, R. A. F., Huang, R. J.,
804 Berkemeier, T., Wang, Y., Su, H., Cheng, Y., Pope, F. D., Fu, P., Yao, M., Pohlker,
805 C., Petaja, T., Kulmala, M., Andreae, M. O., Shiraiwa, M., Poschl, U., Hoffmann, T.,
806 and Kalberer, M.: Radical Formation by Fine Particulate Matter Associated with
807 Highly Oxygenated Molecules, *Environ Sci Technol*, 53, 12506-12518,
808 10.1021/acs.est.9b05149, 2019.
- 809 Wang, Y., Zhang, Q., Jiang, J., Zhou, W., Wang, B., He, K., Duan, F., Zhang, Q., Philip,
810 S., and Xie, Y.: Enhanced sulfate formation during China's severe winter haze
811 episode in January 2013 missing from current models, *Journal of Geophysical*
812 *Research: Atmospheres*, 119, 10,425-410,440, 10.1002/2013jd021426, 2014.



- 813 Wang, J., Wang, G., Gao, J., Wang, H., Ren, Y., Li, J., Zhou, B., Wu, C., Zhang, L.,
814 Wang, S., and Chai, F.: Concentrations and stable carbon isotope compositions of
815 oxalic acid and related SOA in Beijing before, during, and after the 2014 APEC,
816 Atmospheric Chemistry and Physics, 17, 981-992, 10.5194/acp-17-981-2017, 2017a.
- 817 Wang, X. K., Hayeck, N., Brüggemann, M., Yao, L., Chen, H. F., Zhang, C., Emmelin,
818 C., Chen, J. M., George, C., and Wang, L.: Chemical Characteristics of Organic
819 Aerosols in Shanghai: A Study by Ultrahigh-Performance Liquid Chromatography
820 Coupled With Orbitrap Mass Spectrometry, Journal of Geophysical Research-
821 Atmospheres, 122, 11703-11722, 10.1002/2017jd026930, 2017b.
- 822 Wang, K., Zhang, Y., Huang, R.-J., Cao, J., and Hoffmann, T.: UHPLC-Orbitrap mass
823 spectrometric characterization of organic aerosol from a central European city
824 (Mainz, Germany) and a Chinese megacity (Beijing), Atmospheric Environment, 189,
825 22-29, 10.1016/j.atmosenv.2018.06.036, 2018.
- 826 Wang, K., Zhang, Y., Huang, R. J., Wang, M., Ni, H., Kampf, C. J., Cheng, Y., Bilde, M.,
827 Glasius, M., and Hoffmann, T.: Molecular Characterization and Source Identification
828 of Atmospheric Particulate Organosulfates Using Ultrahigh Resolution Mass
829 Spectrometry, Environ Sci Technol, 53, 6192-6202, 10.1021/acs.est.9b02628, 2019a.
- 830 Wang, Y., Hu, M., Lin, P., Tan, T., Li, M., Xu, N., Zheng, J., Du, Z., Qin, Y., Wu, Y., Lu,
831 S., Song, Y., Wu, Z., Guo, S., Zeng, L., Huang, X., and He, L.: Enhancement in
832 Particulate Organic Nitrogen and Light Absorption of Humic-Like Substances over
833 Tibetan Plateau Due to Long-Range Transported Biomass Burning Emissions,
834 Environ Sci Technol, 53, 14222-14232, 10.1021/acs.est.9b06152, 2019b.



- 835 Wang, X., Hayeck, N., Brüggemann, M., Abis, L., Riva, M., Lu, Y., Wang, B., Chen, J.,
836 George, C., and Wang, L.: Chemical Characteristics and Brown Carbon
837 Chromophores of Atmospheric Organic Aerosols Over the Yangtze River Channel:
838 A Cruise Campaign, *Journal of Geophysical Research: Atmospheres*, 125,
839 10.1029/2020jd032497, 2020.
- 840 Win, M. S., Zeng, J., Yao, C., Zhao, M., Xiu, G., Xie, T., Rao, L., Zhang, L., Lu, H., Liu,
841 X., Wang, Q., and Lu, S.: Sources of HULIS-C and its relationships with trace
842 metals, ionic species in PM_{2.5} in suburban Shanghai during haze and non-haze days,
843 *Journal of Atmospheric Chemistry*, 77, 63-81, 10.1007/s10874-020-09404-7, 2020.
- 844 Wong, J. P. S., Nenes, A., and Weber, R. J.: Changes in Light Absorptivity of Molecular
845 Weight Separated Brown Carbon Due to Photolytic Aging, *Environ Sci Technol*, 51,
846 8414-8421, 10.1021/acs.est.7b01739, 2017.
- 847 Wong, J. P. S., Tsagkaraki, M., Tsiodra, I., Mihalopoulos, N., Violaki, K., Kanakidou,
848 M., Sciare, J., Nenes, A., and Weber, R. J.: Effects of Atmospheric Processing on the
849 Oxidative Potential of Biomass Burning Organic Aerosols, *Environ Sci Technol*, 53,
850 6747-6756, 10.1021/acs.est.9b01034, 2019.
- 851 Wu, G., Wan, X., Gao, S., Fu, P., Yin, Y., Li, G., Zhang, G., Kang, S., Ram, K., and
852 Cong, Z.: Humic-Like Substances (HULIS) in Aerosols of Central Tibetan Plateau
853 (Nam Co, 4730 m asl): Abundance, Light Absorption Properties, and Sources,
854 *Environ Sci Technol*, 52, 7203-7211, 10.1021/acs.est.8b01251, 2018a.
- 855 Wu, Z., Wang, Y., Tan, T., Zhu, Y., Li, M., Shang, D., Wang, H., Lu, K., Guo, S., Zeng,
856 L., and Zhang, Y.: Aerosol Liquid Water Driven by Anthropogenic Inorganic Salts:



857 Implying Its Key Role in Haze Formation over the North China Plain, *Environmental*
858 *Science & Technology Letters*, 5, 160-166, 10.1021/acs.estlett.8b00021, 2018b.

859 Yu, L., Smith, J., Laskin, A., George, K. M., Anastasio, C., Laskin, J., Dillner, A. M.,
860 and Zhang, Q.: Molecular transformations of phenolic SOA during photochemical
861 aging in the aqueous phase: competition among oligomerization, functionalization,
862 and fragmentation, *Atmospheric Chemistry and Physics*, 16, 4511-4527,
863 10.5194/acp-16-4511-2016, 2016.

864 Yu, X., Yu, Q., Zhu, M., Tang, M., Li, S., Yang, W., Zhang, Y., Deng, W., Li, G., Yu, Y.,
865 Huang, Z., Song, W., Ding, X., Hu, Q., Li, J., Bi, X., and Wang, X.: Water Soluble
866 Organic Nitrogen (WSON) in Ambient Fine Particles Over a Megacity in South
867 China: Spatiotemporal Variations and Source Apportionment, *Journal of*
868 *Geophysical Research: Atmospheres*, 122, 10.1002/2017jd027327, 2017.

869 Yuan, W., Huang, R. J., Yang, L., Ni, H., Wang, T., Cao, W., Duan, J., Guo, J., Huang,
870 H., and Hoffmann, T.: Concentrations, optical properties and sources of humic-like
871 substances (HULIS) in fine particulate matter in Xi'an, Northwest China, *Sci Total*
872 *Environ*, 789, 147902, 10.1016/j.scitotenv.2021.147902, 2021.

873 Zeng, Y., Shen, Z., Takahama, S., Zhang, L., Zhang, T., Lei, Y., Zhang, Q., Xu, H., Ning,
874 Y., Huang, Y., Cao, J., and Rudolf, H.: Molecular Absorption and Evolution
875 Mechanisms of PM 2.5 Brown Carbon Revealed by Electrospray Ionization Fourier
876 Transform–Ion Cyclotron Resonance Mass Spectrometry During a Severe Winter
877 Pollution Episode in Xi'an, China, *Geophysical Research Letters*, 47,
878 10.1029/2020gl087977, 2020.



- 879 Zeng, Y. L., Ning, Y. L., Shen, Z. X., Zhang, L. M., Zhang, T., Lei, Y. L., Zhang, Q., Li,
880 G. H., Xu, H. M., Ho, S. S. H., and Cao, J. J.: The Roles of N, S, and O in Molecular
881 Absorption Features of Brown Carbon in PM_{2.5} in a Typical Semi-Arid Megacity in
882 Northwestern China, *J Geophys Res-Atmos*, 126, 2021.
- 883 Zhang, J., Liu, L., Xu, L., Lin, Q., Zhao, H., Wang, Z., Guo, S., Hu, M., Liu, D., Shi, Z.,
884 Huang, D., and Li, W.: Exploring wintertime regional haze in northeast China: role of
885 coal and biomass burning, *Atmospheric Chemistry and Physics*, 20, 5355-5372,
886 10.5194/acp-20-5355-2020, 2020.
- 887 Zhang, L., Wang, G., Wang, J., Wu, C., Cao, C., and Li, J.: Chemical composition of
888 fine particulate matter and optical properties of brown carbon before and during
889 heating season in Xi'an, *Journal of Earth Environment*, 8, 451-458, 2017.
- 890 Zhang, Q., Worsnop, D. R., Canagaratna, M. R., and Jimenez, J. L.: Hydrocarbon-like
891 and oxygenated organic aerosols in Pittsburgh: insights into sources and processes of
892 organic aerosols, *Atmospheric Chemistry and Physics*, 5, 3289-3311, 10.5194/acp-5-
893 3289-2005, 2005.
- 894 Zhang, Y.-L., El-Haddad, I., Huang, R.-J., Ho, K.-F., Cao, J.-J., Han, Y., Zotter, P.,
895 Bozzetti, C., Daellenbach, K. R., Slowik, J. G., Salazar, G., Prévôt, A. S. H., and
896 Szidat, S.: Large contribution of fossil fuel derived secondary organic carbon to water
897 soluble organic aerosols in winter haze in China, *Atmospheric Chemistry and
898 Physics*, 18, 4005-4017, 10.5194/acp-18-4005-2018, 2018.
- 899 Zhang, T., Shen, Z., Zeng, Y., Cheng, C., Wang, D., Zhang, Q., Lei, Y., Zhang, Y., Sun,
900 J., Xu, H., Ho, S. S. H., and Cao, J.: Light absorption properties and molecular
901 profiles of HULIS in PM_{2.5} emitted from biomass burning in traditional "Heated



902 Kang" in Northwest China, *Sci Total Environ*, 776, 146014,
903 10.1016/j.scitotenv.2021.146014, 2021.

904 Zhong, M. and Jang, M.: Dynamic light absorption of biomass-burning organic carbon
905 photochemically aged under natural sunlight, *Atmospheric Chemistry and Physics*,
906 14, 1517-1525, 10.5194/acp-14-1517-2014, 2014.

907 Zhu, C. S., Cao, J. J., Huang, R. J., Shen, Z. X., Wang, Q. Y., and Zhang, N. N.: Light
908 absorption properties of brown carbon over the southeastern Tibetan Plateau, *Sci*
909 *Total Environ*, 625, 246-251, 10.1016/j.scitotenv.2017.12.183, 2018.

910 Zou, C., Li, M., Cao, T., Zhu, M., Fan, X., Peng, S., Song, J., Jiang, B., Jia, W., Yu, C.,
911 Song, H., Yu, Z., Li, J., Zhang, G., and Peng, P. a.: Comparison of solid phase
912 extraction methods for the measurement of humic-like substances (HULIS) in
913 atmospheric particles, *Atmospheric Environment*, 225, 117370,
914 10.1016/j.atmosenv.2020.117370, 2020.

915

916



917 **Table 1.** Formular number of potential BrC chromophores and the intensity ratios of each group of
 918 potential BrC in total potential BrC and each group of total identified formulas, respectively.

Samples	Elemental compositions	Number	ESI-		Elemental compositions	Number	ESI+	
			$\text{Int}_C/\text{Int}_{\text{BrC}}$	$\text{Int}_{\text{BrC},i}/\text{Int}_{\text{bulk}}$			$\text{Int}_C/\text{Int}_{\text{BrC}}$	$\text{Int}_{\text{BrC},i}/\text{Int}_{\text{bulk}}$
Clean-I	CHO-	424	0.48	0.25	CHO+	263	0.37	0.07
	CHON-	773	0.46	0.53	CHON+	480	0.56	0.15
	CHOS-	63	0.03	0.05	CHN+	79	0.07	0.56
	CHONS-	43	0.03	0.08	all in ESI+	822		0.11
	all in ESI-	1303		0.26				
Haze-I	CHO-	356	0.44	0.21	CHO+	244	0.29	0.09
	CHON-	791	0.50	0.45	CHON+	614	0.62	0.22
	CHOS-	43	0.03	0.03	CHN+	94	0.09	0.39
	CHONS-	39	0.03	0.07	all in ESI+	952		0.16
	all in ESI-	1229		0.22				
Haze-II	CHO-	444	0.45	0.26	CHO+	333	0.34	0.06
	CHON-	941	0.49	0.49	CHON+	595	0.56	0.13
	CHOS-	67	0.03	0.03	CHN+	89	0.1	0.48
	CHONS-	78	0.03	0.07	all in ESI+	1017		0.10
	all in ESI-	1530		0.25				
Clean-II	CHO-	391	0.46	0.27	CHO+	234	0.38	0.09
	CHON-	707	0.48	0.59	CHON+	462	0.56	0.18
	CHOS-	64	0.03	0.05	CHN+	75	0.06	0.57
	CHONS-	49	0.03	0.10	all in ESI+	771		0.13
	all in ESI-	1211		0.29				

919 Int_C : the intensity of each group of identified potential BrC;

920 Int_{BrC} : the sum intensity of identified potential BrC;

921 Int_{Bulk} : the sum intensity of each group of total identified formulas.



922
 923
 924
 925
 926
 927
 928
 929
 930
 931
 932
 933
 934
 935
 936
 937
 938
 939
 940
 941
 942
 943
 944
 945
 946
 947
 948
 949
 950

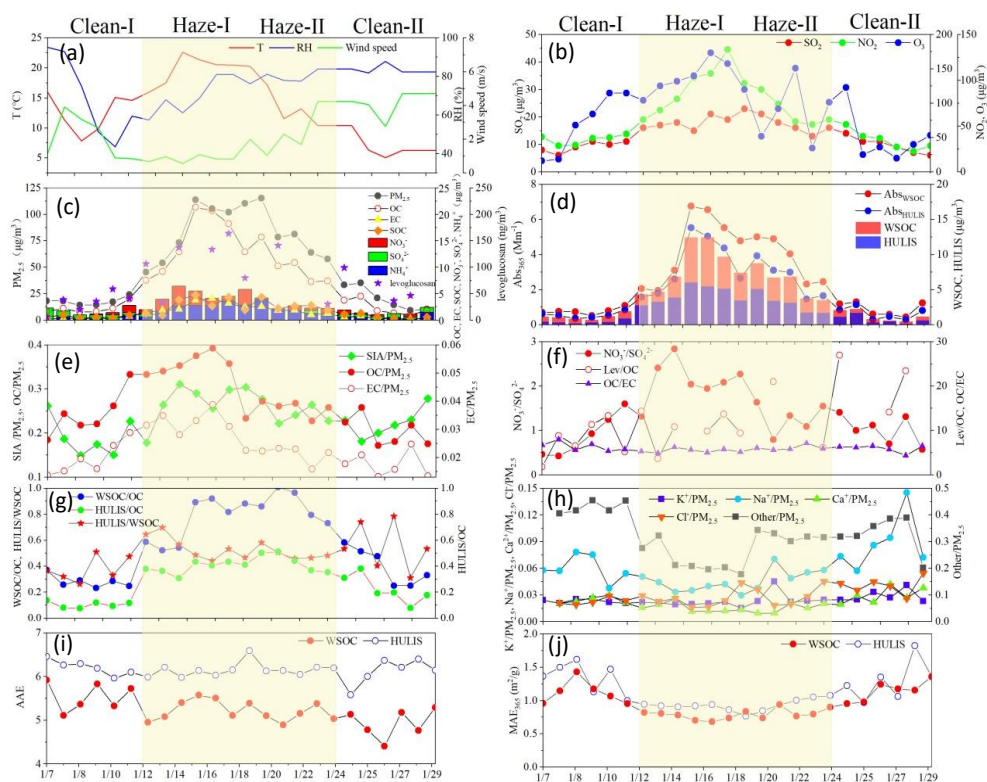


Figure 1. Temporal variation in meteorological parameters, concentrations of chemical composition, and optical properties (Abs_{365} , MAE_{365} , and AAE) of water-soluble BrC in the $PM_{2.5}$ samples.



951

952

953

954

955

956

957

958

959

960

961

962

963

964

965

966

967

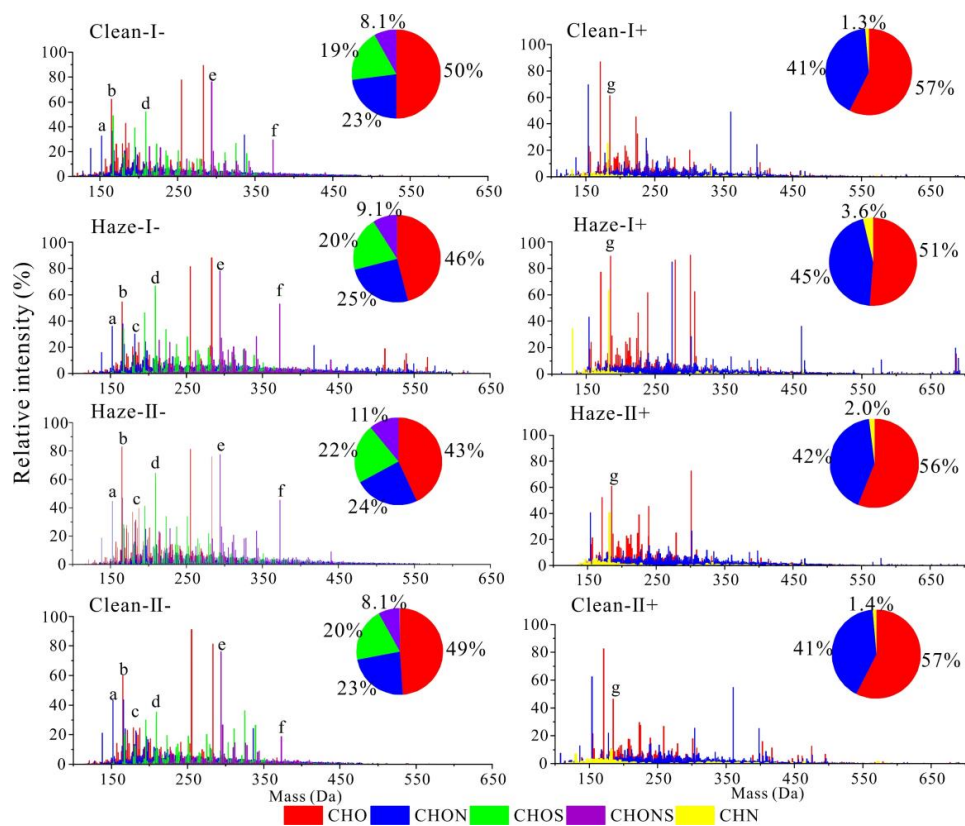
968

969

970

971

972



973

Figure 2. Mass spectra of HULIS detected in ESI- and ESI+ modes during the haze

974

process. The pie charts represent the intensity percent of different compound groups.

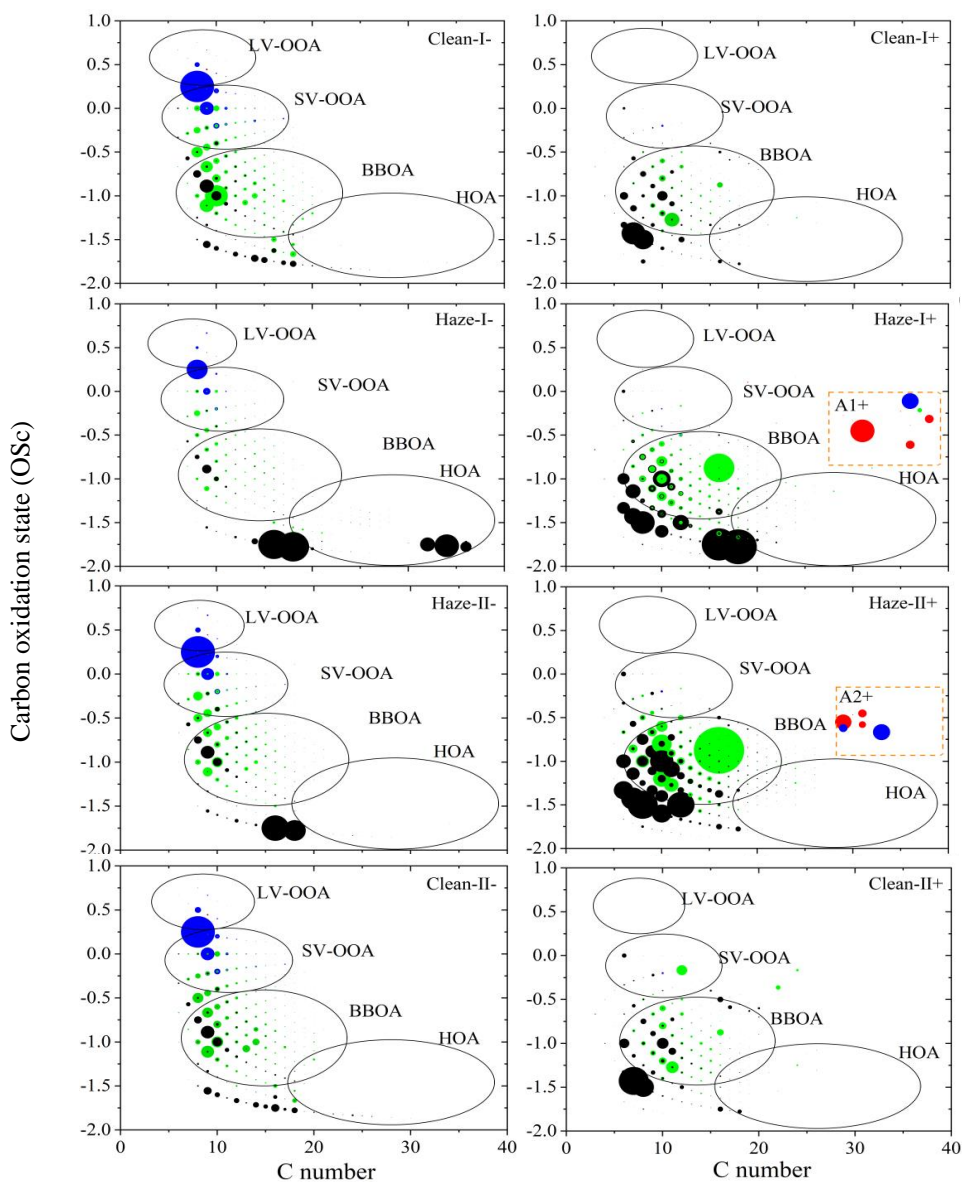
975

976

977



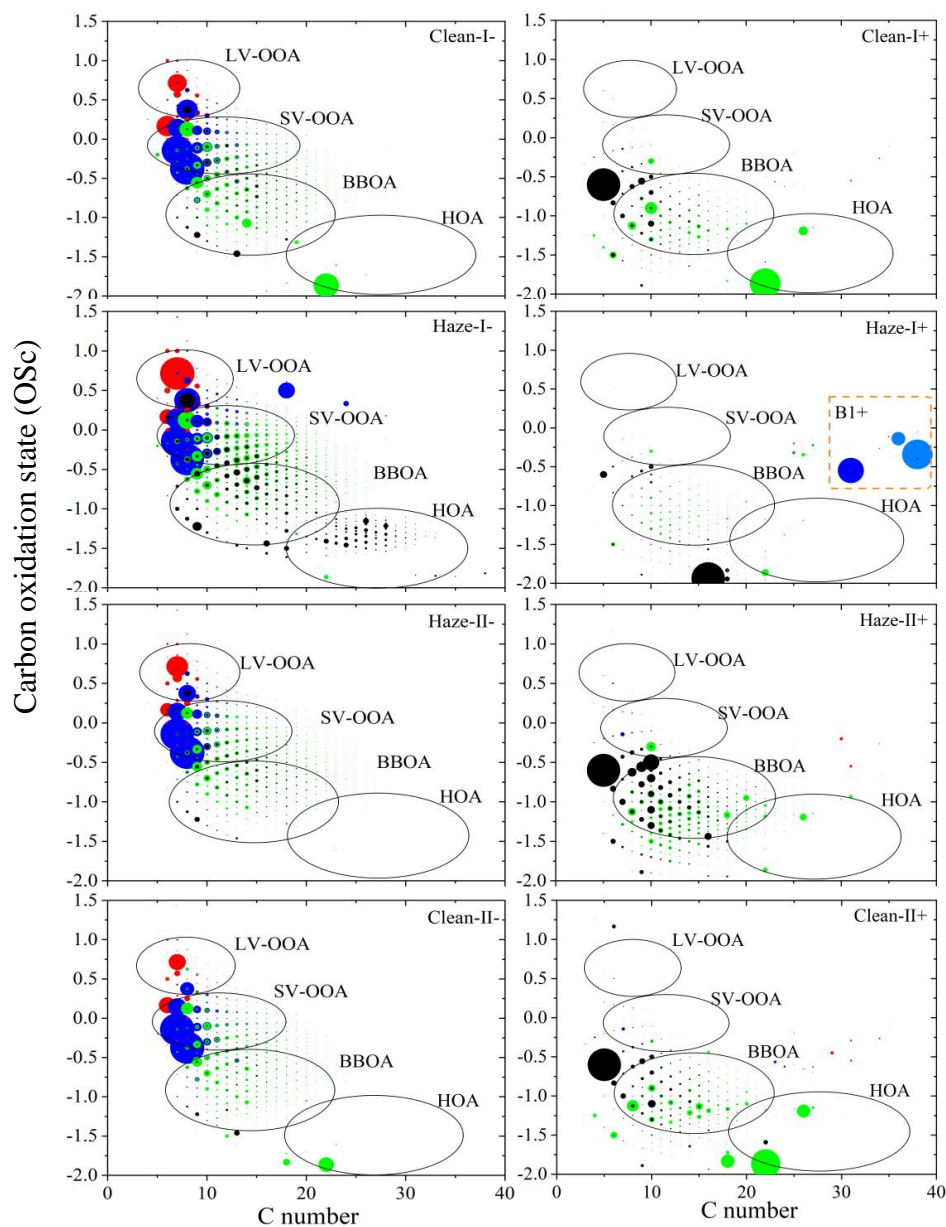
978
979
980
981
982
983
984
985
986
987
988
989
990
991
992
993
994
995
996
997
998
999
1000
1001
1002
1003
1004
1005
1006
1007
1008
1009



1010 **Figure 3.** Carbon oxidation state (OSc) plots for CHO- and CHO+. Formulas with black,
1011 green, blue, and red are assigned to aliphatic (AI = 0), olefinic ($0 < AI < 0.5$), aromatic
1012 ($0.5 \leq AI < 0.67$), and condensed aromatic ($AI \geq 0.67$) species (Koch and Dittmar, 2006),
1013 respectively.



1014
1015
1016
1017
1018
1019
1020
1021
1022
1023
1024
1025
1026
1027
1028
1029
1030
1031
1032
1033
1034
1035
1036
1037
1038
1039
1040
1041
1042
1043
1044
1045



1046 **Figure 4.** Carbon oxidation state (OSc) plots for CHON- and CHON+. Formulas with
1047 black, green, blue, and red are assigned to aliphatic ($AI = 0$), olefinic ($0 < AI < 0.5$),
1048 aromatic ($0.5 \leq AI < 0.67$), and condensed aromatic ($AI \geq 0.67$) species (Koch and Dittmar,
1049 2006), respective.



1050
1051
1052
1053
1054
1055
1056
1057
1058
1059
1060
1061
1062
1063
1064
1065
1066
1067
1068
1069
1070

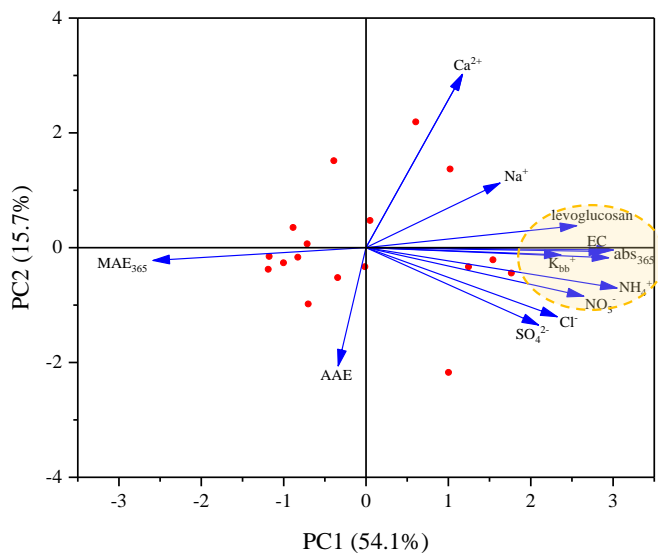


Figure 5. Principal component analysis results for the optical properties of HULIS and chemical compositions of PM_{2.5}.